Atmospheric Science Letters

RMetS Royal Meteorological Society

RESEARCH ARTICLE OPEN ACCESS

Assessment of the ECMWF Data Assimilation System Using Radiosonde Profiles During Atmospheric River Events Over Western Europe

Alexandre M. Ramos[1] | Alexander Lemburg[1] | David A. Lavers[2] | Ricardo Tomé[3] | Joaquim G. Pinto[1]

[1]Institute of Meteorology and Climate Research Troposphere Research (IMKTRO), Karlsruhe Institute of Technology (KIT), Karlsruhe, Germany | [2]ECMWF, Reading, UK | [3]Instituto Dom Luiz, Faculdade de Ciências, Universidade de Lisboa, Lisbon, Portugal

Correspondence: Alexandre M. Ramos (alexandre.ramos@kit.edu)

Received: 12 January 2026 | **Revised:** 14 April 2026 | **Accepted:** 1 May 2026

Keywords: atmospheric rivers | data assimilation | ECMWF IFS | radiosondes | Western Europe

ABSTRACT

Atmospheric Rivers (ARs) are one of the key elements in explaining the occurrence of extreme precipitation and floods in mid-latitudes. Despite the recognised importance of ARs, few studies have systematically evaluated how a weather forecast model captures AR conditions affecting western Europe. Using radiosonde observations from different sites across western Europe, this study evaluates the specific humidity, wind speed and moisture flux in the data assimilation system of the ECMWF Integrated Forecasting System (IFS) for the extended winter of 2020/2021 with a particular focus on landfalling ARs. Results indicate a systematic underestimation of specific humidity, wind and moisture flux in the IFS, particularly during more intense moisture flux events. The most significant negative biases of the IFS were observed in the boundary layer (1000–900 hPa) and lower free troposphere (900–700 hPa), coinciding with the core region of moisture flux. Wind speed was generally underestimated, with the largest errors occurring in the boundary layer at locations with complex topography. In addition, as expected, the assimilation of radiosonde profiles reduced short-range forecast errors. The results highlight the current limitations in forecasting AR intensity and location and show the importance of in situ observations to improve the forecast of high-impact weather events.

1 | Introduction

High-impact weather (HIW) is among the most significant natural hazards affecting western Europe (Pinto et al. 2019). These events occur most frequently during the boreal winter and include heavy precipitation, flooding and intense windstorms (Wernli et al. 2002; Ulbrich et al. 2009; Fink et al. 2009; Hewson and Neu 2015). The cyclones generally responsible for HIW are characterised by so-called conveyor belts, which describe the atmospheric streams within a cyclone (Schultz et al. 2019). In particular, the Warm Conveyor Belt (WCB; Carlson 1980) transports humid air ahead of the cold front, rising towards the cyclone centre. Associated with cyclones and the WCB are Atmospheric Rivers (ARs, Dacre et al. 2015, 2019; Ralph et al. 2018), which are defined as long, narrow and transient corridors of intense horizontal water vapour transport. The moisture transported within an AR may subsequently feed a WCB which can lead to prolonged heavy precipitation and increased flood risk (e.g., Pfahl et al. 2014; Ferreira et al. 2025), resulting in large socio-economic impacts (e.g., Doiteau et al. 2021; Michel et al. 2021; López-Martí et al. 2025). For example, over the Iberian Peninsula, ARs contributed to extreme rainfall and flooding in different river basins (Ramos et al. 2015; Eiras-Barca et al. 2018; Ferreira et al. 2025). In addition, the United Kingdom has also experienced AR-driven events causing widespread flooding (Lavers et al. 2011), most notably during the winter storms of 2013/2014 (Priestley et al. 2017). Furthermore, there is evidence also of an

interdependency between cyclone intensity and the presence of an AR (Eiras-Barca et al. 2018).

Since ARs are relatively narrow corridors of intense horizontal water vapour transport, their landfall position plays a crucial role in determining the location of potential extreme precipitation events (Ramos et al. 2015; Demirdjian et al. 2020; Ralph et al. 2020). Therefore, accurate forecasting of the location, timing and intensity of ARs is crucial to estimate potential impacts (Lavers, Ralph, et al. 2020). An objective assessment of forecast accuracy at different lead times is of paramount importance, particularly regarding AR landfall position and intensity and this was previously undertaken using Integrated Vapour Transport (IVT) (e.g., Ramos et al. 2020). Despite previous research diagnosing ARs with IVT, less is known about how weather forecast models skilfully represent the vertical structure of ARs, particularly during extreme events (e.g., Lavers, Ingleby, et al. 2020; Zheng et al. 2021).

One approach to assess the vertical structure of ARs is by using observed radiosonde profiles, which deliver high-resolution measurements of pressure, temperature, humidity and wind. These in situ observations are normally released from a set of synoptic weather stations across the globe at specific times and provide crucial details on the vertical atmospheric structure for weather forecasting (e.g., Bauer et al. 2015; Lavers, Ingleby, et al. 2020). A second approach is to use dropsondes which can be released from research aircraft during observational campaigns, such as in the Atmospheric River Reconnaissance (AR Recon) campaign over the North Pacific (Ralph et al. 2020). These dropsonde observations—which are similar to radiosonde profiles—have been shown to be useful for forecast model diagnostics (e.g., Lavers, Ingleby, et al. 2020) and can improve the forecasts of landfalling ARs and therefore the precipitation over western United States (Wang et al. 2026).

Despite the recognised importance of ARs (Lavers, Ralph, et al. 2020), there are almost no systematic evaluations of short-range forecast performance using radiosonde observations in Europe. This is an important question as it may help inform observational targeting in field campaigns in Europe like the North Atlantic Waveguide, Dry Intrusion and Downstream Impact Campaign (NAWDIC, https://www.nawdic.kit.edu) which took place in January/February 2026. NAWDIC focused on cyclone development over the North Atlantic and the interaction between Dry Intrusions and the marine boundary layer, as well as downstream impacts. The aim of this study is to evaluate the short-range forecast performance of the European Centre for Medium-Range Weather Forecasts (ECMWF) Integrated Forecasting System (IFS) data assimilation system using radiosonde observations of specific humidity, wind and moisture flux during the extended winter of 2020/2021 across western Europe. The analysis considers multiple landfalling AR events, allowing assessment of model performance across different locations. Specifically, we address the following research questions: (i) what errors in the IFS are typically found in humidity, wind and moisture flux during AR events? and (ii) in which tropospheric layers are the largest moisture flux and associated errors found? The remainder of this paper is organised as follows: Section 2 describes the data and methods, including the radiosonde observations and the model evaluation framework while Section 3 presents the main results. Finally in Section 4, we present the discussion and the conclusions.

2 | Data and Methods

2.1 | Radiosonde Observations and the ECMWF IFS

We use radiosonde observations (specific humidity and wind speed) retrieved from ECMWF at several launch sites along the western coast of Europe (Table 1). The site selection was based on data completeness (more than 90% availability in winter 2020/21) and on their representativeness of regions where ARs most frequently make landfall (Eiras-Barca et al. 2018). Radiosondes report humidity as dew point temperature (Td). Within the ECMWF processing chain, specific humidity is derived for assimilation using vapour pressure computed from Td with the Sonntag saturation vapour pressure (SVP) formulation (Ingleby 2017).

In this study, the long-window data assimilation system in the ECMWF IFS is considered, which has two 12-h assimilation windows: from 0900 to 2100 UTC and from 2100 to 0900 UTC. Within each window, a four-dimensional variational (4D-Var)

TABLE 1 | List of the radiosonde stations considered in this study, including their WMO identifier, geographic coordinates (latitude and longitude), elevation and percentage of missing data over the winter of 2020/2021 and the corresponding 85th percentile IVT threshold ($kg\,m^{-1}\,s^{-1}$), computed from the nearest ERA5 grid point over the climatological extended winter period 1979–2020.

	WMO ID	Latitude °	Longitude °	Elevation m	Missing %	IVT 85th ($kg\,m^{-1}\,s^{-1}$)
Stavanger, NO	1415	58.87	5.67	9	1.6%	238.04
Camborne, UK	3808	50.22	−5.33	87	4.7%	336.71
Valentia, IE	3953	51.94	−10.24	25	0%	351.05
Brest, FR	7110	48.44	−4.41	95	0%	334.85
Bordeaux, FR	7510	44.83	−0.69	54	1.9%	283.45
La Coruna, ES	8001	43.37	−8.42	67	1.6%	325.42
Lisbon, PT	8536	38.78	−9.13	123	8.0%	274.99
Huelva, ES	8383	37.28	−6.91	20	3.3%	241.93

assimilation method is used (Rabier et al. 2000), combining short-range or 'background forecasts' (3–15 h, also referred to as the 'first-guess' (FG) forecasts) with all available observations, including the radiosonde profiles. This process yields a new 'analysis' (AN) that represents the best estimate of the atmospheric state, nominally at 0000 UTC and 1200 UTC, respectively. These analyses then serve as input for the early-delivery assimilation cycle, which provides the initial conditions for the operational IFS forecasts. For this study, the observed radiosonde profiles, as well as the corresponding first-guess and analysis profiles were retrieved from the ECMWF archive for each 12-h long-window data assimilation window between 1 October 2020 and 31 March 2021. Balloon drift is accounted for by comparing the observations with the nearest model grid point along the balloon ascent trajectory. During this time, IFS Cycle 47r1 was in operation at ECMWF (ECMWF 2022).

2.2 | Forecast Evaluation and Moisture Flux Calculation

The considered time period provides a large enough sample to evaluate the model biases of the analysis and first-guess throughout the troposphere from the near-surface to 300 hPa. We use the convention of the forecast community by computing the forecast-minus-observation statistic (Lavers et al. 2023) and the biases are evaluated for the specific humidity, wind speed and moisture flux magnitude. We also undertake a conditional evaluation to investigate AR events by splitting the extended winter 2020/2021 into two samples: all days (00UTC and 12UTC) and only those for the more intense IVT time steps. Intense IVT time steps at a given location are defined as those times at which the instantaneous IVT (at either 00UTC and/or 12UTC) exceeds the local 85th percentile of IVT computed over the ECMWF reanalysis version 5 (ERA5, Hersbach et., 2020) climatological extended winter period 1979–2024. For each radiosonde location, the 85th percentile threshold was calculated using the ERA5 grid point closest to the station and the corresponding threshold values are listed in Table 1. The frequency of Intense IVT time steps range over the different locations range from ~16% to 22% (Figure S1). The mean sea-level pressure (MSLP) and vertically integrated water vapour flux from the ERA5 reanalysis (Hersbach et al. 2020) were retrieved from the Climate Data Store (https://cds.climate.copernicus.eu).

At each station, the radiosonde observations and model data are finally pooled into 25 hPa wide vertical bins. This strategy results in an average of about 4500 individual values per vertical bin for all considered days and about 550 values for the more intense IVT days, respectively.

For an easier comparison of all evaluated sites, we further aggregate the data levels into three atmospheric layers defined as follows: 900–1000 hPa, which corresponds primarily to the winter-time planetary boundary layer (PBL); 700–900 hPa, which mostly corresponds to the lower free troposphere (LFT; the winter-time PBL might extend beyond 900 hPa in individual cases, but stays below 900 hPa on average); and 300–700 hPa, which corresponds to the upper free troposphere (UFT). Traditionally, the core of the AR is considered to be between the surface and 700 hPa (Ralph et al. 2017).

We test the statistical significance of the respective model biases per vertical bin via classic bootstrapping (resampling from the full sample with replacement) with 10,000 repetitions. When the 95% confidence interval of the bootstrapped distributions overlaps zero, the respective bias in the given vertical bin is considered to be insignificant. We apply the same procedure also to the difference of biases between analysis and first guess in order to assess whether data assimilation leads to a significantly improved representation of the atmospheric state.

3 | Results

3.1 | AR Event Case Study for Brest Radiosonde Site

As a case study, we examine one AR event at the Brest radiosonde site during the extended winter of 2020/2021. This event highlights the vertical structure of moisture flux and wind biases, providing context for understanding model performance under intense IVT conditions. On 21 December 2020 at 12:00 UTC, the Brest region was under the influence of an intense AR (IVT above 500 $kg\,m^{-1}\,s^{-1}$) associated with a deep cyclone to the west of Europe at about 45° N, 30° W (Figure 1a). ARs are often characterised by strong IVT gradients from the core of the AR towards its edges (Ralph et al. 2018), which also occurred when this AR made landfall in the Brest region (Figure 1b). For this particular date, we compare the vertical profiles of both AN and the FG with observations from the radiosonde ascent at Brest (Figure 1c–e). The AN shows a slight overestimation (0.5 g/kg) of specific humidity up to approximately 925 hPa. However, from this level up to 700 hPa, the FG and AN considerably underestimate (2.5 and 1 g/kg, respectively) specific humidity, with FG showing a more pronounced underestimation (Figure 1c). Regarding wind speed (Figure 1d), the FG and AN show an overestimation (between 2 and 3 m/s) below 875 hPa, after which AN is in very good agreement with observations up to 775 hPa, most likely resulting from the data assimilation procedure. At higher levels, from 650 hPa upwards, the FG is generally closer to the observations than AN.

Moreover, we also derived the magnitude of the moisture flux at each available pressure level (see Section 2.2) and the results are shown in Figure 1e. This particular radiosonde ascent is characterised by an overestimation of the flux in the lower levels (below 900 hPa), which is higher in the AN (~75 $(g\,kg^{-1})\,(m\,s^{-1})$) than in the FG (~10 $(g\,kg^{-1})\,(m\,s^{-1})$). There is a particular layer, between 825 and 725 hPa, where the FG significantly underestimates (50 $(g\,kg^{-1})\,(m\,s^{-1})$) the moisture flux. This is mainly due to larger errors in the specific humidity (Figure 1c). Finally, the accuracy of the model increases above 725 hPa with respect to the observations. In summary, this case study shows that for this AR landfall event, the ECMWF IFS struggled to represent its vertical structure, with a strong underestimation of moisture fluxes in the lower free troposphere, particularly in the FG.

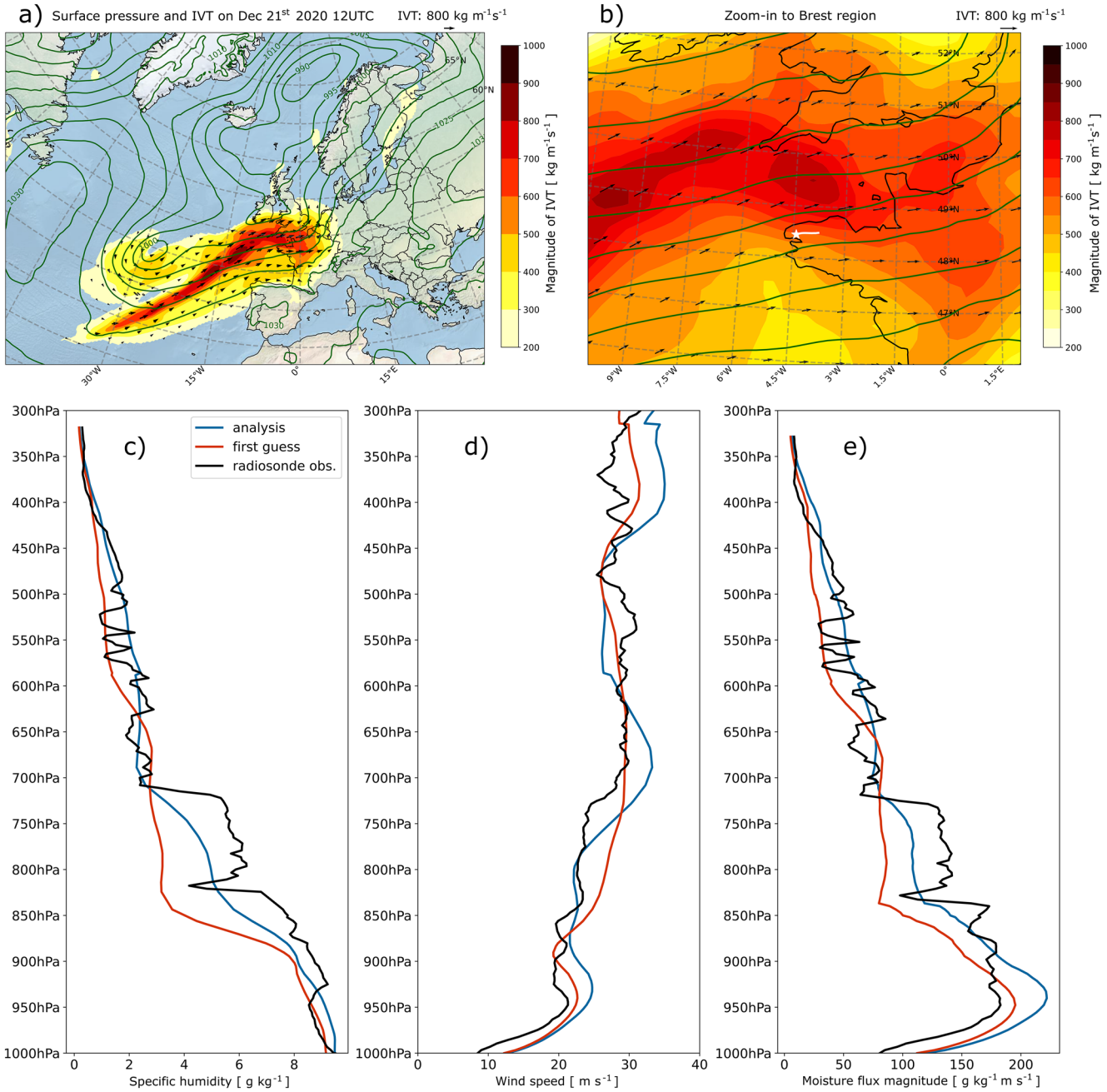

FIGURE 1 | Case study of an AR affecting Brest on 21 December 2020 12UTC. The first row features a synoptic overview depicting ERA5-based surface pressure fields (contour lines) and IVT (vectors, magnitude as shading) for the Euro-Atlantic region (a) and a zoom-in to the Brest region (b). The second row presents vertical profiles of the ECMWF IFS analysis and first-guess compared to radiosonde observations for specific humidity (c), wind speed (d) and the magnitude of the moisture flux (e).

3.2 | Vertical Bias Structure at Brest Radiosonde Site

To evaluate the vertical bias of the ECMWF forecasts, we analyse all radiosonde observations at Brest during the extended winter of 2020/2021. The evaluation analysis includes both the full winter season dataset and a subset corresponding to intense IVT events at this location, allowing a representative assessment of the model's performance across different atmospheric layers. By comparing the respective errors of the FG and AN, we can assess potential improvements of the model state by the assimilation of observations. In this regard, Figure 2 shows the bias and standard deviation of the forecasts-minus-observations of specific humidity, wind speed and moisture flux for each 25 hPa interval bin at Brest; these statistics assess the systematic (mean) and random errors, respectively. First, as is expected, the biases are generally higher for the FG (red) than for the AN (blue), meaning that the model fits more closely to the observations following the data assimilation step. Second, the biases are consistently larger during more intense IVT days (lighter blue/red shades), particularly for the FG. Focusing on the individual variables, the specific humidity profile (Figure 2a) shows a small but consistent dry bias in the model which is much more pronounced in the FG compared to AN, particularly in the lower

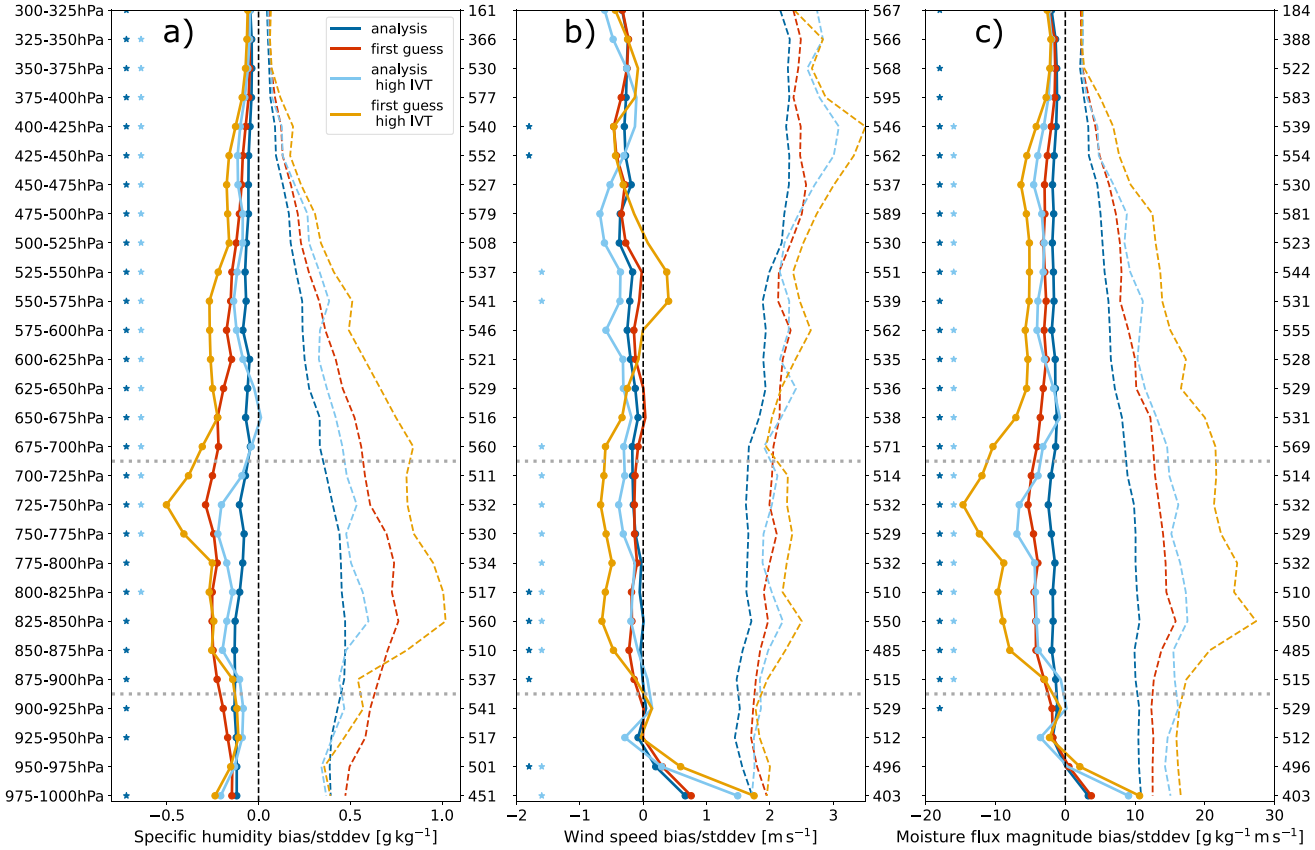

FIGURE 2 | Vertical profiles of errors of ECMWF IFS AN (blueish colours) and FG (reddish colours) at Brest, France, for the period October 2020 to March 2021. For each 25-hPa bin, solid lines depict the bias and dashed lines denote the standard deviation. Darker colours present errors for the entire extended winter while lighter colours show errors only for more intense IVT days. Filled circles within the solid lines denote that the respective mean bias is statistically distinguishable from zero with 95% confidence according to a bootstrapping procedure with 10,000 repetitions. Asterisk symbols highlight vertical levels for which the bias of analysis has a statistically significantly lower magnitude compared to the first guess (dark blue: Entire period, light blue: Only intense IVT days). On the right-hand y-axis, the numbers denote the number of available observations per bin for more intense IVT days. Dashed horizontal lines corresponds to the three atmospheric layers defined as follows: Between 900–1000 hPa to planetary boundary layer (PBL); between 700–900 hPa, lower free troposphere (LFT); and between 300–700 hPa, upper free troposphere (UFT).

free troposphere. During more intense IVT days, the dry bias is exacerbated in the FG (peaking at 0.5 g/kg), especially between 775 and 700 hPa. For the same layer, the AN shows a significantly lower bias. The standard deviation of the error in each bin for specific humidity is much higher than the bias between 950 and 600 hPa. This pattern suggests that the model exhibits both systematic and random errors in correctly representing lower-tropospheric moisture, particularly during more intense IVT days. At higher altitudes, specific humidity values are very low, so even small absolute differences can produce large and potentially misleading bias values and we therefore interpret these results with caution.

Regarding wind speed (Figure 2b), the model tends to overestimate (peaking at 2 m/s) wind speed in the boundary layer and underestimate (up to −0.75 m/s) it in the lower and upper free troposphere. For the moisture flux on the pressure levels (Figure 2c), the AN generally captures the vertical profile reasonably well for the extended winter 2020/2021. In the boundary layer, the biases are predominantly driven by wind, whereas above 900 hPa they are mainly caused by the specific humidity errors. Once again, during more intense IVT events, both the FG and AN exhibit larger biases, especially in the 700–900 hPa layer and in the boundary layer near the surface, reflecting the model's difficulty in representing moisture transport values at the top and above the PBL in more extreme conditions. Nonetheless, the magnitude of the bias is significantly smaller in AN than in FG in nearly all vertical levels with the exception of the lower half of the PBL.

3.3 | Europe-Wide Evaluation of AN and FG Biases

We extend the bias assessment to all eight radiosonde sites across western Europe, considering all days and high IVT time steps during the extended winter of 2020/2021. This multi-site, multi-event analysis enables a robust evaluation of spatial variability in model performance, highlighting locations and pressure layers. Figure 3 provides a synthesis of the main results for both the AN and FG for specific humidity, wind speed and moisture flux across all radiosonde locations considered (detailed vertical profiles, as in Figure 2, are provided in Figures S2–S8). For specific humidity, the results generally show that the IFS has an underestimation throughout the 2020/2021 winter in the boundary layer (Figure 3a), with a larger underestimation during the more intense IVT days. For Brest and Bordeaux, the model underestimation reaches the highest values (−0.35 g/kg),

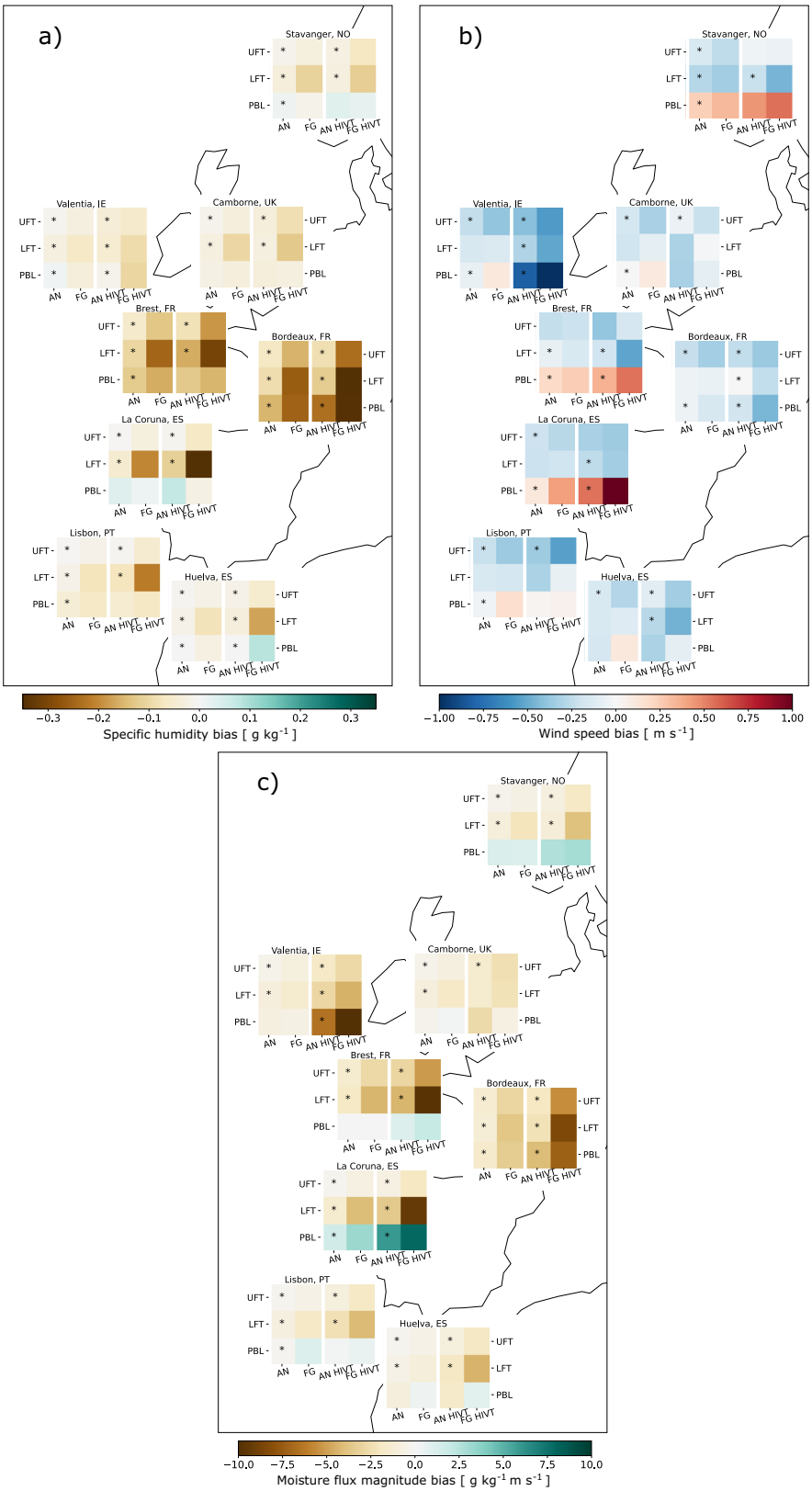

FIGURE 3 | Overview of average model biases across Europe in the extended winter season 2020/2021 for the quantities moisture (a), wind speed (b) and moisture flux magnitude (c). For each of the evaluated sites, biases are displayed for the three atmospheric layers planetary boundary layer (PBL, 1000–900 hPa), lower free troposphere (LFT; 900–700 hPa) and upper free troposphere (UFT; 700–300 hPa). The two left columns denote biases for AN and FG for the entire extended winter, respectively, whereas the two columns on the right display biases of AN and FG for more intense IVT days. Asterisk symbols highlight atmospheric layers for which the bias of analysis has a statistically significantly lower magnitude compared to the first guess.

while at the northernmost location, Stavanger, a slight model overestimation is found (< 0.05 g/kg). In the FG, the biases are generally significantly larger, indicating that the radiosonde observations (and other assimilated observations) improve the model's representation, particularly under AR conditions. The model generally struggles to represent wind speed in the boundary layer (Figure 3b), with a particularly strong overestimation (> 0.75 m/s) at three locations (La Coruña, Brest and Stavanger) and underestimates (−1 m/s) in Valentia. Once again, the biases are larger under AR conditions. We find the model analysis (AN) is improved significantly through assimilation of observations at most sites, particularly during more intense IVT days (except at Camborne and Huelva, where FG shows a smaller bias than AN).

Focusing on the lower and upper free troposphere, the results are broadly comparable, particularly for specific humidity (Figure 3a). At all locations there is an underestimation of specific humidity, which is generally significantly more pronounced in the FG than in the AN, indicating an improvement following the assimilation of observations. This effect is even more pronounced in La Coruna, Bordeaux and Brest, where the largest biases (< −0.3 g/kg) are found which are higher during the more intense IVT days. Caution is required when interpreting the results for specific humidity in the upper free troposphere, because its absolute values are much lower compared with the boundary layer. For wind speed in the lower and upper free troposphere (Figure 3b), the results are consistent across all locations, showing an underestimation (not lower than −0.75 m/s) of wind speed, which is larger during the more intense IVT days. At most sites, the AN shows a smaller bias compared to the FG, suggesting that the data assimilation step reduces the model error. However, this effect is not as noticeable as for specific humidity.

For the moisture flux in the boundary layer (Figure 3c), the spatial pattern is heterogeneous and depends on the relative contributions of specific humidity and wind at each site. At several locations (notably Bordeaux, Valentia and Camborne), the boundary-layer moisture flux is underestimated (peaking at −10 ($g\,kg^{-1}$) ($m\,s^{-1}$) in Valentia), driven primarily by the pronounced underestimation of specific humidity. By contrast, an overestimation of boundary layer flux occurs at sites where near-surface winds are overestimated (e.g., La Coruña around 10 ($g\,kg^{-1}$) ($m\,s^{-1}$) and Stavanger ~2.5 ($g\,kg^{-1}$) ($m\,s^{-1}$)), indicating that dynamical errors can offset thermodynamic errors. For most sites, biases tend to be larger during more intense IVT days and significantly more pronounced in the FG than in the AN, signifying that the assimilation of radiosonde observations (and other assimilated observations) improves the model's representation of boundary layer moisture flux. For the moisture flux in the lower and upper free troposphere (Figure 3c), the model shows a systematic underestimation across most locations, particularly during the more intense IVT days. This underestimation is most pronounced at La Coruña, Bordeaux and Brest, where both the magnitude of the flux and the associated biases are largest. At all sites, biases in the AN are significantly reduced compared to the FG.

4 | Discussion and Conclusion

This study has evaluated the short-range forecast performance of the ECMWF IFS long-window data assimilation system at radiosonde sites across western Europe during the extended winter of 2020/2021. By assessing the systematic (mean) and random errors of the specific humidity, wind and moisture-flux using radiosonde observations, the main findings are:

i. The results indicate a general underestimation of specific humidity, wind speed and moisture flux in the IFS compared to the radiosonde profiles, with larger biases in the FGs than in the AN, especially during more intense IVT days. The assimilation of radiosonde profiles (and other observation sources) improves the representation of the moisture flux, particularly under AR conditions, although considerable random errors persist across most layers.

ii. For the boundary layer (1000–900 hPa), an underestimation is generally found for specific humidity, with the largest underestimation at Brest and Bordeaux, while Stavanger shows an overestimation. For wind speed, the IFS tends to underestimate winds at most locations, although overestimation occurs at northern or coastal sites with complex topography (e.g., La Coruña, Brest and Stavanger). These errors are reflected in the moisture flux, where a clear overestimation is seen in Stavanger and La Coruna.

iii. For the lower free troposphere (900–700 hPa), a negative bias, or model underestimation, is seen at all locations for specific humidity, wind speed and moisture flux. Together with the boundary layer, it exhibits the largest biases and corresponds to the region contributing most to atmospheric moisture flux. During more intense IVT days, the strongest biases are indeed found between the surface and 700 hPa.

iv. In the upper free troposphere (700–300 hPa), the wind speed is generally underestimated in the FG across all observation sites, with the largest biases occurring during more intense IVT days and near the upper-tropospheric jet around 300 hPa. Moreover, the specific humidity drops sharply with height, so moisture-flux biases in this layer should be interpreted cautiously.

The results show potentially larger model errors during HIW events driven by ARs, particularly when errors in specific humidity and wind speed vertical profiles lead to biases in moisture flux. The strong variability of forecast errors across Europe aligns with previous work highlighting substantial regional differences in terms of IFS error characteristics (Frame et al. 2015). Boundary layer (1000–900 hPa) errors at La Coruña, Brest and Stavanger may be linked to orography and/or land sea contrasts (Thuburn and Staniforth 2019). The 700–900 hPa layer shows the strongest biases, consistent with its critical role in moisture flux in ARs (Ralph et al. 2018). The location of the strongest errors during more intense IVT days, between the surface and 700 hPa, corresponds to the AR core region and is consistent with previous findings from in situ and modelling studies (Ralph et al. 2017; Lavers, Ingleby, et al. 2020; Gorodetskaya et al. 2020).

The combined biases in the moisture flux emphasise the joint thermodynamic and dynamical contributions to model

limitations in representing AR-related transport processes (Zavadoff and Kirtman 2020). In particular, biases in low-level moisture during intense IVT conditions may be linked to the representation of vertical moisture transport and boundary-layer mixing (Schäfler et al. 2024), which can strongly influence the distribution of water vapour within the AR. Furthermore, small positional or intensity errors associated with the jet stream can lead to systematic wind and moisture flux biases, given the strong coupling between ARs, pressure gradients and upper-level jet dynamics (Lavers et al. 2023; Schäfler et al. 2020).

Doyle et al. (2014) and Schäfler and Harnisch (2015) showed that latent heat release from water vapour condensation within ARs can modify the dynamical evolution of the associated cyclone, thereby affecting the intensity and predictability of the AR. In this context, inaccuracies in condensation processes or microphysical parameterisations may also contribute to the vertical structure of the observed humidity biases (Krüger et al. 2022). Improvements seen in the AN are consistent with earlier studies reporting enhanced forecast skill when assimilating radiosonde data (Ingleby et al. 2018; Krüger et al. 2024; Schäfler et al. 2024).

Our results highlight that the AN generally exhibits small biases across all examined fields, in part because radiosonde observations were assimilated. In contrast, many of these biases reappear in the FG forecasts, particularly during the intense IVT events. This result indicates that the remaining systematic errors could originate from model limitations, such as the grid spacing and representativeness. While our study cannot fully diagnose the exact physical mechanisms responsible, this behaviour is important for guiding future model improvements.

Several caveats of this study should be acknowledged. Radiosonde coverage is limited both spatially and temporally, meaning that model performance could only be assessed at specific locations and times which may reflect local characteristics. Moreover, because this analysis focuses on a single winter season (2020/2021), the results may not fully capture the interannual variability of AR characteristics and associated model performance. This is partly because the IFS is typically updated once per year (ECMWF 2025), so differences between model cycles may affect the representation of AR related processes. Lavers, Ralph, et al. (2020) note that improvements in AR forecasts may require systematic reconnaissance or improved modelling, such as those undertaken in the AR Recon campaign and proposed in the NAWDIC campaign.

This study provides one of the first Europe-wide evaluations of short-range IFS performance against radiosonde observations during landfalling ARs, offering a framework for understanding the capability of modelling systems to capture HIW events such as ARs. The extensive observations from the North Atlantic taken during the NAWDIC campaign will allow for further studies, such as investigating the representativeness of the radiosonde observations and they will also contribute to a better representation and potentially higher predictive skill of the cyclones in forecasting systems like the IFS. Furthermore, the Brest region benefited from enhanced radiosonde coverage, complemented by the deployment of a ground-based mobile observation platform (NAWDIC-KITcube), which will provide an ideal testbed for the framework introduced in this study.

Ultimately, these observations can be key to help improve our understanding of the processes driving biases in moisture and wind fields in AR regions, improving the representation of initial conditions in numerical models and potentially increasing forecast skill of HIW events over Europe.

Author Contributions

Alexandre M. Ramos: conceptualization, methodology, writing – original draft, writing – review and editing, funding acquisition, investigation, visualization, formal analysis. **Ricardo Tomé:** writing – review and editing, methodology. **Alexander Lemburg:** writing – original draft, writing – review and editing, visualization, formal analysis, methodology. **David A. Lavers:** conceptualization, data curation, methodology, writing – review and editing. **Joaquim G. Pinto:** writing – review and editing, funding acquisition, methodology.

Acknowledgements

We thank the German Climate Computer Centre (DKRZ, Hamburg) for computer and storage resources. We thank the European Centre for Medium-Range Weather Forecasts (ECMWF) for accessing the forecast and analysis products. We also thank two anonymous reviewers for their helpful and constructive comments. Open Access funding enabled and organized by Projekt DEAL.

Funding

This work was developed partially under the framework of the project 'Improving Atmospheric River forecasts with enhanced observations in moisture source regions (NAWDIC-AR)' funded by the German Research Foundation (DFG, grant number: 564641009). A.M.R. received support from the Helmholtz Changing Earth program. J.G.P. thanks the AXA Research Fund for support. A.L. and J.G.P. are funded by the German Federal Ministry of Research, Technology and Space (BMFTR) research program ClimXtreme II: A5 DesAttHeat (01LP2322A). D.L. was supported by the Copernicus Climate Change Service, which is implemented by the European Centre for Medium-Range Weather Forecasts (ECMWF) on behalf of the European Union. R.T. is supported the Portuguese Fundação para a Ciência e a Tecnologia (FCT) I.P./MCTES through national funds (PIDDAC): LA/P/0068/2020-https://doi.org/10.54499/LA/P/0068/2020, UID/50019/2025, https://doi.org/10.54499/UID/PRR/50019/2025, UID/PRR2/50019/2025.

Conflicts of Interest

The authors declare no conflicts of interest.

Data Availability Statement

The data used are available through the ECMWF archive (https://www.ecmwf.int/en/forecasts/access-forecasts/access-archive-datasets).

References

Bauer, P., A. Thorpe, and G. Brunet. 2015. "The Quiet Revolution of Numerical Weather Prediction." *Nature* 525: 47–55. https://doi.org/10.1038/nature14956.

Carlson, T. N. 1980. "Airflow Through Midlatitude Cyclones and the Comma Cloud Pattern." *Monthly Weather Review* 108: 1498–1509.

https://doi.org/10.1175/1520-0493(1980)108<1498:ATMCAT>2.0.CO;2.

Dacre, H. F., P. A. Clark, O. Martinez-Alvarado, M. A. Stringer, and D. A. Lavers. 2015. "How Do Atmospheric Rivers Form?" *Bulletin of the American Meteorological Society* 96: 1243–1255. https://doi.org/10.1175/BAMS-D-14-00031.1.

Dacre, H. F., O. Martínez-Alvarado, and C. O. Mbengue. 2019. "Linking Atmospheric Rivers and Warm Conveyor Belt Airflows." *Journal of Hydrometeorology* 20: 1183–1196. https://doi.org/10.1175/JHM-D-18-0175.1.

Demirdjian, R., J. D. Doyle, C. A. Reynolds, J. R. Norris, A. C. Michaelis, and F. M. Ralph. 2020. "A Case Study of the Physical Processes Associated With the Atmospheric River Initial-Condition Sensitivity From an Adjoint Model." *Journal of the Atmospheric Sciences* 77: 691–709. https://doi.org/10.1175/JAS-D-19-0155.1.

Doiteau, B., M. Dournaux, N. Montoux, and J.-L. Baray. 2021. "Atmospheric Rivers and Associated Precipitation Over France and Western Europe: 1980–2020 Climatology and Case Study." *Atmosphere* 12, no. 8: 1075. https://doi.org/10.3390/atmos12081075.

Doyle, J. D., C. Amerault, C. A. Reynolds, and P. A. Reinecke. 2014. "Initial Condition Sensitivity and Predictability of a Severe Extratropical Cyclone Using a Moist Adjoint." *Monthly Weather Review* 142: 320–342. https://doi.org/10.1175/MWR-D-13-00201.1.

ECMWF. 2022. Implementation of IFS Cycle 47r1, Reading, UK. https://confluence.ecmwf.int/display/FCST/Implementation+of+IFS+Cycle+47r1.

ECMWF. 2025. *Integrated Forecasting System (IFS) Cycles Overview*. European Centre for Medium-Range Weather Forecasts. https://www.ecmwf.int/en/forecasts/documentation-and-support/changes-ecmwf-model.

Eiras-Barca, J., A. M. Ramos, J. G. Pinto, R. M. Trigo, M. L. R. Liberato, and G. Miguez-Macho. 2018. "The Concurrence of Atmospheric Rivers and Explosive Cyclogenesis in the North Atlantic and North Pacific Basins." *Earth System Dynamics* 9: 91–102. https://doi.org/10.5194/esd-9-91-2018.

Ferreira, T. M., R. M. Trigo, T. H. Gaspar, J. G. Pinto, and A. M. Ramos. 2025. "The Record-Breaking Precipitation Event of December 2022 in Portugal." *Natural Hazards and Earth System Sciences* 25: 609–623. https://doi.org/10.5194/nhess-25-609-2025.

Fink, A. H., T. Brücher, V. Ermert, A. Krüger, and J. G. Pinto. 2009. "The European Storm Kyrill in January 2007: Synoptic Evolution, Meteorological Impacts and Some Considerations With Respect to Climate Change." *Natural Hazards and Earth System Sciences* 9: 405–423. https://doi.org/10.5194/nhess-9-405-2009.

Frame, T. H., J. Methven, N. M. Roberts, and H. A. Titley. 2015. "Predictability of Frontal Waves and Cyclones." *Weather and Forecasting* 30: 1291–1302. https://doi.org/10.1175/WAF-D-15-0039.1.

Gorodetskaya, I. V., T. Silva, H. Schmithüsen, and N. Hirasawa. 2020. "Atmospheric River Signatures in Radiosonde Profiles and Reanalyses at the Dronning Maud Land Coast, East Antarctica." *Advances in Atmospheric Sciences* 37: 455–476. https://doi.org/10.1007/s00376-020-9221-8.

Hersbach, H., B. Bell, P. Berrisford, et al. 2020. "The ERA5 Global Reanalysis." *Quarterly Journal of the Royal Meteorological Society* 146: 1999–2049. https://doi.org/10.1002/qj.3803.

Hewson, T. D., and U. Neu. 2015. "Cyclones, Windstorms and the IMILAST Project." *Tellus. Series A, Dynamic Meteorology and Oceanography* 67: 27128. https://doi.org/10.3402/tellusa.v67.27128.

Ingleby, B. 2017. *An Assessment of Different Radiosonde Types 2015/2016. ECMWF Technical Memorandum No. 807*. European Centre for Medium-Range Weather Forecasts. https://doi.org/10.21957/0nje0wpsa.

Ingleby, B., L. Isaksen, T. Kral, T. Haiden, and M. Dahoui. 2018. "Improved Use of Atmospheric In Situ Data." *ECMWF Newsletter* 155: 20–25. https://doi.org/10.21957/cf724bi05s.

Krüger, K., A. Schäfler, M. Weissmann, and G. C. Craig. 2024. "Influence of Radiosonde Observations on the Sharpness and Altitude of the Midlatitude Tropopause in the ECMWF IFS." *Weather and Climate Dynamics* 5: 491–509. https://doi.org/10.5194/wcd-5-491-2024.

Krüger, K., A. Schäfler, M. Wirth, M. Weissmann, and G. C. Craig. 2022. "Vertical Structure of the Lower-Stratospheric Moist Bias in the ERA5 Reanalysis and Its Connection to Mixing Processes." *Atmospheric Chemistry and Physics* 22: 15559–15577.

Lavers, D. A., R. P. Allan, E. F. Wood, G. Villarini, D. J. Brayshaw, and A. J. Wade. 2011. "Winter Floods in Britain Are Connected to Atmospheric Rivers." *Geophysical Research Letters* 38: L23803. https://doi.org/10.1029/2011GL049783.

Lavers, D. A., N. B. Ingleby, A. C. Subramanian, et al. 2020. "Forecast Errors and Uncertainties in Atmospheric Rivers." *Weather and Forecasting* 35: 1447–1458. https://doi.org/10.1175/WAF-D-20-0049.1.

Lavers, D. A., F. M. Ralph, D. S. Richardson, and F. Pappenberger. 2020. "Improved Forecasts of Atmospheric Rivers Through Systematic Reconnaissance, Better Modelling, and Insights on Conversion of Rain to Flooding." *Communications Earth & Environment* 1: 39. https://doi.org/10.1038/s43247-020-00042-1.

Lavers, D. A., R. D. Torn, C. Davis, D. S. Richardson, F. M. Ralph, and F. Pappenberger. 2023. "Forecast Evaluation of the North Pacific Jet Stream Using AR Recon Drop Windsondes." *Quarterly Journal of the Royal Meteorological Society* 149, no. 756: 3044–3063. https://doi.org/10.1002/qj.4545.

López-Martí, F., L. Wu, G. Messori, and A. Rutgersson. 2025. "Moisture Sources Throughout the Life Cycle of an Atmospheric River: Storm Dennis Case Study." *Journal of Geophysical Research: Atmospheres* 130: e2024JD042876. https://doi.org/10.1029/2024JD042876.

Michel, C., A. Sorteberg, S. Eckhardt, C. Weijenborg, A. Stohl, and M. Cassiani. 2021. "Characterization of the Atmospheric Environment During Extreme Precipitation Events Associated With Atmospheric Rivers in Norway—Seasonal and Regional Aspects." *Weather and Climate Extremes* 34: 100370. https://doi.org/10.1016/j.wace.2021.100370.

Pfahl, S., E. Madonna, M. Boettcher, H. Joos, and H. Wernli. 2014. "Warm Conveyor Belts in the ERA-Interim Dataset (1979–2010). Part II: Moisture Origin and Relevance for Precipitation." *Journal of Climate* 27: 27–40. https://doi.org/10.1175/JCLI-D-13-00223.1.

Pinto, J. G., F. Pantillon, P. Ludwig, et al. 2019. "From Atmospheric Dynamics to Insurance Losses: An Interdisciplinary Workshop on European Storms." *Bulletin of the American Meteorological Society* 100: ES175–ES178. https://doi.org/10.1175/BAMS-D-19-0026.1.

Priestley, M. D., J. G. Pinto, H. F. Dacre, and L. C. Shaffrey. 2017. "The Role of Cyclone Clustering During the Stormy Winter of 2013/2014." *Weather* 72: 187–192. https://doi.org/10.1002/wea.3025.

Rabier, F., H. Järvinen, E. Klinker, J.-F. Mahfouf, and A. Simmons. 2000. "The ECMWF Operational Implementation of Four-Dimensional Variational Assimilation. Part I: Experimental Results With Simplified Physics." *Quarterly Journal of the Royal Meteorological Society* 126: 1143–1170. https://doi.org/10.1002/qj.49712656415.

Ralph, F. M., F. Cannon, V. Tallapragada, et al. 2020. "West Coast Forecast Challenges and Development of Atmospheric River Reconnaissance." *Bulletin of the American Meteorological Society* 101: E1357–E1377. https://doi.org/10.1175/BAMS-D-19-0183.1.

Ralph, F. M., M. D. Dettinger, M. M. Cairns, T. J. Galarneau, and J. Eylander. 2018. "Defining "Atmospheric River": How the Glossary

of Meteorology Helped Resolve a Debate." *Bulletin of the American Meteorological Society* 99: 837–839. https://doi.org/10.1175/BAMS-D-17-0157.1.

Ralph, F. M., S. F. Iacobellis, P. J. Neiman, et al. 2017. "Dropsonde Observations of Total Water Vapor Transport Within North Pacific Atmospheric Rivers." *Journal of Hydrometeorology* 18: 2577–2596. https://doi.org/10.1175/JHM-D-17-0036.1.

Ramos, A. M., P. M. Sousa, E. Dutra, and R. M. Trigo. 2020. "Predictive Skill for Atmospheric Rivers in the Western Iberian Peninsula." *Natural Hazards and Earth System Sciences* 20: 877–888. https://doi.org/10.5194/nhess-20-877-2020.

Ramos, A. M., R. M. Trigo, M. L. Liberato, and R. Tomé. 2015. "Daily Precipitation Extreme Events in the Iberian Peninsula and Its Association With Atmospheric Rivers." *Journal of Hydrometeorology* 16: 579–597. https://doi.org/10.1175/JHM-D-14-0103.1.

Schäfler, A., and F. Harnisch. 2015. "Impact of the Inflow Moisture on the Evolution of a Warm Conveyor Belt." *Quarterly Journal of the Royal Meteorological Society* 141: 299–310. https://doi.org/10.1002/qj.2360.

Schäfler, A., B. Harvey, J. Methven, et al. 2020. "Observation of Jet Stream Winds During NAWDEX and Characterization of Systematic Meteorological Analysis Errors." *Monthly Weather Review* 148: 2889–2907.

Schäfler, A., K. Krüger, A. Oertel, J. Quinting, and S. Raveh-Rubin. 2024. "Indication for Biases in Dry Intrusions and the Marine Boundary Layer Over the Azores in ECMWF Short-Term Forecasts and Analyses." *Geophysical Research Letters* 51: e2024GL109601. https://doi.org/10.1029/2024GL109601.

Schultz, D. M., S. Pfahl, and H. Wernli. 2019. "Cyclone Conveyor Belts: A Review." *Monthly Weather Review* 147: 1071–1097. https://doi.org/10.1175/MWR-D-18-0377.1.

Thuburn, J., and A. Staniforth. 2019. "Uncertainty in the Representation of Orography in Weather and Climate Models." *Journal of Advances in Modeling Earth Systems* 11: 1991–2008. https://doi.org/10.1029/2019MS001661.

Ulbrich, U., G. C. Leckebusch, and J. G. Pinto. 2009. "Extra-Tropical Cyclones in the Present and Future Climate: A Review." *Theoretical and Applied Climatology* 96: 117–131. https://doi.org/10.1007/s00704-008-0083-8.

Wang, J., D. A. Lavers, L. Delle Monache, et al. 2026. "Impacts of Atmospheric River Reconnaissance Dropsondes on ECMWF Integrated Forecasting System Precipitation Forecasts." *Quarterly Journal of the Royal Meteorological Society* 152, no. 774: e70019. https://doi.org/10.1002/qj.70019.

Wernli, H., S. Dirren, M. A. Liniger, and M. Zillig. 2002. "Dynamical Aspects of the Life Cycle of the Winter Storm 'Lothar' (24–26 December 1999)." *Quarterly Journal of the Royal Meteorological Society* 128: 405–429. https://doi.org/10.1256/003590002321042036.

Zavadoff, B. L., and B. P. Kirtman. 2020. "Dynamic and Thermodynamic Modulators of European Atmospheric Rivers." *Journal of Climate* 33: 4167–4185. https://doi.org/10.1175/JCLI-D-19-0601.1.

Zheng, M., L. Delle Monache, B. D. Cornuelle, et al. 2021. "Improved Forecast Skill Through the Assimilation of Dropsonde Observations From the Atmospheric River Reconnaissance Program." *Journal of Geophysical Research: Atmospheres* 126: e2021JD034967. https://doi.org/10.1029/2021JD034967.

Supporting Information

Additional supporting information can be found online in the Supporting Information section. **Figure S1:** Temporal distribution and frequency of extreme Integrated Vapor Transport (IVT) events across the eight study locations (October 2020–March 2021). Percentages indicate the relative occurrence of intense IVT time steps at each station. **Figure S2:** Vertical profiles of errors of ECMWF IFS AN (blueish colours) and FG (reddish colours) at Stavanger, Norway, for the period October 2020 to March 2021. For each 25-hPa bin, solid lines depict the bias and dashed lines denote the standard deviation. Darker colours present errors for the entire extended winter while lighter colours show errors only for more intense IVT days. Filled circles within the solid lines denote that the respective mean bias is statistically distinguishable from zero with 95% confidence according to a bootstrapping procedure with 10,000 repetitions. Asterisk symbols highlight vertical levels for which the bias of analysis has a statistically significantly lower magnitude compared to the first guess (dark blue: entire period, light blue: only intense IVT days). On the right-hand *y*-axis, the numbers denote the number of available observations per bin for more intense IVT days. Dashed horizontal lines corresponds to the three atmospheric layers defined as follows: between 900–1000 hPa to planetary boundary layer (PBL); between 700–900 hPa, lower free troposphere (LFT; and between 300–700 hPa, upper free troposphere (UFT). **Figure S3:** As Figure S2, but for Camborne (United Kingdom). **Figure S4:** As Figure S2, but for Valentia (Ireland). **Figure S5:** As Figure S2, but for Bordeaux (France). **Figure S6:** As Figure S2, but for La Coruna (Spain). **Figure S7:** As Figure S2, but for Huelva (Spain). **Figure S8:** As Figure S2, but for Lisbon (Portugal).